ORIGINAL ARTICLE

In Vivo Wireless Brain Stimulation via Non-invasive and Targeted Delivery of Magnetoelectric Nanoparticles

Tyler Nguyen[1,2,3,4] · Jianhua Gao[1,2] · Ping Wang[5] · Abhignyan Nagesetti[5] · Peter Andrews[2] · Sehban Masood[2] · Zoe Vriesman[2] · Ping Liang[6] · Sakhrat Khizroev[5] · Xiaoming Jin[1,2]

Abstract

Wireless and precise stimulation of deep brain structures could have important applications to study intact brain circuits and treat neurological disorders. Herein, we report that magnetoelectric nanoparticles (MENs) can be guided to a targeted brain region to stimulate brain activity with a magnetic field. We demonstrated the nanoparticles' capability to reliably evoke fast neuronal responses in cortical slices ex vivo. After fluorescently labeled MENs were intravenously injected and delivered to a targeted brain region by applying a magnetic field gradient, a magnetic field of low intensity (350–450 Oe) applied to the mouse head reliably evoked cortical activities, as revealed by two-photon and mesoscopic imaging of calcium signals and by an increased number of c-Fos expressing cells after stimulation. Neither brain delivery of MENs nor the magnetic stimulation caused significant increases in astrocytes and microglia. Thus, MENs could enable a non-invasive and contact-less deep brain stimulation without the need of genetic manipulation.

Keywords Noninvasive brain stimulation · Nanoparticles · Calcium imaging · Two-photon · Neuroinflammation

Introduction

In the last two decades, noninvasive brain stimulation techniques have made important contributions to the understanding of brain neurophysiology and treatment of neurological diseases. The two most common forms of noninvasive brain stimulation used clinically are transcranial magnetic stimulation (TMS) and transcranial direct current stimulation (tDCS) [1–3]. However, they have relatively low spatial and temporal precisions, which greatly diminish their efficacy and application. For example, regular TMS has a spatial resolution of 3–5 cm and a depth of penetration of ~ 1–1.5 cm, which allows for stimulating a cortical gyrus [4, 5]. tDCS also has a relatively low spatial resolution and limited effects on deep brain structures [4, 6, 7]. More recent approaches such as optogenetics [8, 9], magneto-thermal brain stimulation [10, 11], and ultrasound-based transcranial stimulations [12] have improved in ways that were limited in tDCS and TMS, but present drawbacks including the requirement of genetic modifications, invasive brain delivery of particles, or brain tissue damage due to high release of thermal energy.

The concept of using magnetoelectric nanoparticles (MENs) for brain stimulation was first proposed in 2012 [13] and was later demonstrated with MENs-mediated modulation of brain EEG activity [14] with the most recent attempt by Kozielski et al. to demonstrate to enhance thalamic neuronal activity in vitro (preprinted) [15]. They used $CoFe_2O_4$-$BaTiO_3$ MENs due to their relatively strong magneto-electric (ME) effect owing to the strain-induced

✉ Xiaoming Jin
   xijin@iupui.edu

   Tyler Nguyen
   ptnguyen@iu.edu

1   Indiana Spinal Cord and Brain Injury Research Group, Stark Neuroscience Research Institute & Department of Anatomy, Cell Biology and Physiology, Indiana University School of Medicine, Indianapolis, IN, USA

2   Indiana Spinal Cord and Brain Injury Research Group, Stark Neuroscience Research Institute & Department of Neurological Surgery, Indiana University School of Medicine, Indianapolis, IN, USA

3   Department of Anesthesia, Indiana University School of Medicine, Indianapolis, IN, USA

4   Medical Neuroscience Program, Indiana University School of Medicine, Indianapolis, IN, USA

5   Department of Electrical and Computer Engineering, College of Engineering, University of Miami, Miami, FL, USA

6   Cellular Nanomed Inc, Irvine, CA, USA

coupling between the magnetostrictive cobalt ferrite cores and piezoelectric barium titanate shells. The nanoparticles can be injected into a vein or via intranasal administration [16], forced to cross the blood–brain barrier (BBB) and consequently localized to a target region by applying a magnetic field gradient. When exposed to a relatively low magnetic field (<~1000 Oe), the MEN's cobalt ferrite (CoFe$_2$O$_4$) core experiences non-zero strain due to the magnetostrictive effect. Owing to the ME coupling, this strain propagates through the lattice matched interface to the adjacent barium titanate (BaTiO$_3$) shell, which in turn induces a local electric field (on the order of 1000 V/m) due to the piezoelectric effect [14]. In this way, magnetic brain stimulation using MENs (MENs-MS) can be achieved with a magnetic field intensity that is much lower than what is used for typical TMS [17]. The unique properties of MENs, due to their small size (~ 30 nm) and the ME effect not displayed by any other nanoparticles known to date, may provide significant improvements over currently used techniques in efficacy and tissue penetration for noninvasive brain stimulation. However, to date, no direct effect of MENs on stimulating neurons in smaller brain regions and/or a large neural network has been convincingly demonstrated.

In the current study, we developed a non-invasive technique using MENs to wirelessly stimulate cortical neuronal activity. Using ex vivo and in vivo fluorescent and two-photon imaging techniques, we showed that MENs can be drawn to cross the BBB and localized to a target cortical region without any apparent signs of neuroinflammation. By activating the MENs with a weak external magnetic field at a specific frequency, we were able to induce cortical activities in individual neurons and in a large neural network in vivo.

Results

MENs synthesis and Characterization

We developed MENs with a core–shell nanostructure, in which the magnetic core was intrinsically coupled to the piezoelectric shell via perfect lattice matching (Fig. 1A). The size of the MENs was on the order of 30 nm. With this new synthesis, we were able to develop MENs with a high ME coefficient of > 5 V/cm/Oe in the frequency range, 0 to 200 Hz, under study. The details of this study have been presented in our recent publications. We developed MENs with a core–shell nanostructure, in which the magnetic core was intrinsically coupled to the piezoelectric shell via perfect lattice matching (Fig. 1A). The size of the MENs was on the order of 30 nm. With this new synthesis, we were able to develop MENs with a high ME coefficient of > 5 V/cm/Oe in the frequency range, 0 to 200 Hz, under study. The details of this study have been presented in our recent publications [18–20].

The coercivity field of the nanoparticles, measured via alternating gradient magnetometry (AGM), was on the order of 400 Oe (Fig. 1B). According to the ME physics described in the aforementioned papers [18], the application of an a.c. magnetic field with a strength of higher than the 400-Oe mark is required to induce the neuromodulation process. It can be noted that for the ME effect to be significant, it is critical to be outside the M-H hysteresis loop, while the coefficient is close to zero when the field is within the loop. Therefore, in this respect, the applied field strength in this frequency range serves as an "On/Off" switch of the modulation. However, for the switch to work,
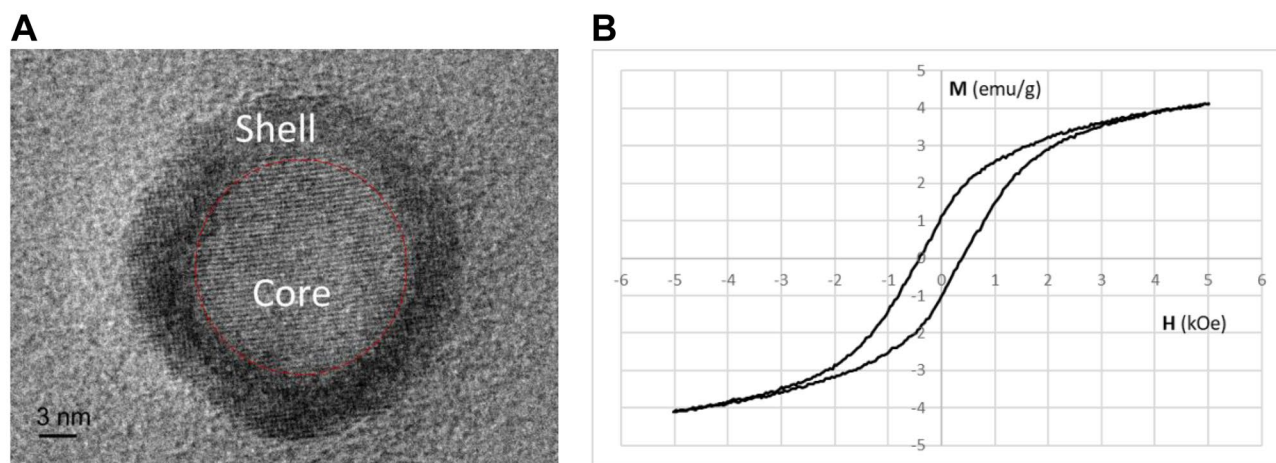

Fig. 1 Transmission electron microscopy (TEM) image and M-H loop of magnetoelectric nanoparticles (MENs). **A** A TEM image demonstrates an almost-perfect lattice matched surface interface between the magnetostrictive core and the piezoelectric shell (shown with broken line) of the coreshell nanostructure. **B** M-H loop, measured with an alternating gradient magnetometer

after each application, the process needs to be properly reset by reversing the polarity of the applied field. That is the reason we work with an a.c. magnetic field.

MENs-MS Induced Neuronal Activity in Cortical Slices Ex Vivo

To assess the effects of MENs-MS on neuronal activity, we used a single pulse (unipolar square pulse at 750–875 Oe, 200-ms duration) of magnetic field and tested the effect in acutely prepared cortical slices from GCaMP6 transgenic mice (Fig. 2A). The mean amplitude of calcium spikes at baseline was 0.127 ± 0.035, which became 0.541 ± 0.056 during magnetic stimulation, and returned to 0.121 ± 0.32 after the magnet was turned off ($p < 0.005$, repeated ANOVA; Fig. 2B). Most of the evoked calcium responses had a short latency period (Fig. 2C), with over 80% of the responses occurring in less than 1 s and 32% of the responses in < 150 ms after the magnetic pulse was turned on.

Intravenous Injection of MENs Followed by Magnetic Delivery to Brain

We used in vivo two-photon imaging to determine how long intravenously injected MENs would be detectable in blood-stream. Immediately after injecting fMENs, we found many fluorescent particles in blood stream of cortical vessels. These particles decreased rapidly over a short period of time (Fig. 3A–B): with the fluorescence intensity in blood stream dropping to about a half in ~15 min and to almost zero in ~30 min after injection (Fig. 3B). This decrease suggested that the optimal time window for applying a magnet for MENs delivery is within ~10 min after intravenous injection of MENs.

We used fMENs to assess the effectiveness of applying permanent magnet for delivering MENs into brain parenchyma. Following intravenous injection of fMENs and application of a conical magnet on mouse head for 20 min (Fig. 3C–D), in vivo two-photon imaging showed that fluorescence signals were visible through cranial windows in mice with fMENs delivery, but not in mice with MENs injection only. The result suggests that the fMENs were drawn by a magnetic field to cross BBB and entered brain parenchyma in vivo (Fig. 3A–B). When the same mice were imaged again 24 h later, signals of fMENs were visible but reduced in the same region (Fig. 3D).

MENs-MS Induced Cortical Neuronal Activity and Network Activity In Vivo

We used in vivo two-photon imaging in GCaMP6 transgenic mice to assess whether MENs-MS would evoke cortical neuronal activity (Fig. 4A–D). In control mice that were injected with saline and followed by MS with a 10-Hz magnetic wave, we found no significant change in mean amplitudes or frequency of calcium spikes (Fig. 4C–D). In mice that were injected with MENs and followed by delivery of MENs and MS with a 10-Hz magnetic wave, we found a dramatic increase in the mean amplitude of calcium spikes (Fig. 4C. F/F_o of 1.50 ± 0.09, 2.37 ± 0.18, and ± 1.36 for baseline, MS-on, and MS-off, respectively, $p < 0.05$, repeated-measures ANOVA, Tukey's HSD) and spike frequency (3.08 ± 0.27 spikes/cell for MS-on vs. 1.96 ± 0.24 for baseline and 1.54 ± 0.25 for MS-off with $p < 0.05$, repeated ANOVA, Tukey's HSD; Fig. 4D) in cortical layer II/III neurons. We found that for every magnetic frequency applied during the stimulation period, a significant increase in somatic calcium spike amplitude occurred (Fig. 4E). The strongest neuronal responses (i.e., the highest average spike amplitude and frequency) were evoked by magnetic waves at 5, 10 and 20 Hz (Fig. 4E, F). Therefore, the 10-Hz frequency was picked as the standard for in vivo stimulation in most of the experiments of our study.

To evaluate the efficacy of brain stimulations over a time period, we gave animals a single MENs delivery and then performed MS and calcium imaging at different time points (Fig. 5). We found a large increase in the amplitude of calcium spikes when MS is applied immediately after MENs delivery (mean F/F_o of 2.7 ± 0.27 vs 1.13 ± 0.07 of baseline, $p < 0.05$, one-way ANOVA, Tukey's HSD; Fig. 5B, D). Neuronal activity could still be stimulated with similar parameters of MS at 24 h after MENs delivery (F/F_o of 2.35 ± 0.28, $p < 0.05$, one-way ANOVA, Tukey's HSD), but not at 72 h after (Fig. 5D. F/F_o of 1.21 ± 0.18, $p > 0.05$, one-way ANOVA). We also found a higher number of active cells after MENs treatment up to 24 h (~90 cells of MENs+MS and 82 cells of 24 h vs. 62 of ms-only baseline; Fig. 5C), and recover to baseline level at 72 h (~55 cells; Fig. 5C). The result suggests that a single delivery of MENs to brain is effective for non-invasive brain stimulation for at least 24 h.

To assess the effect of MENs-MS on global network activity, we applied mesoscopic brain imaging technique to evaluate hemispheric calcium response in GCaMP6 mice (Fig. 6A–F). The epicenter region was defined as the location where a permanent magnet was applied to draw MENs to a local cortical region (Fig. 6A). Application of a 10-Hz magnetic field induced cortical calcium spikes with significantly higher amplitude and varying latencies in the epicenter and contralateral cortex (($\sim F/F_o = 0.23 \pm 0.07$ and 0.26 ± 0.05 for contralateral cortex and epicenter, respectively, compare to baseline 0.07 ± 0.04 and after magnet was turned off 0.05 ± 0.04 $p < 0.05$, repeated ANOVA, Tukey's HSD, Fig. 6B, C). Comparing the responses among the epicenter and different ipsilateral and contralateral cortical regions revealed a highest peak
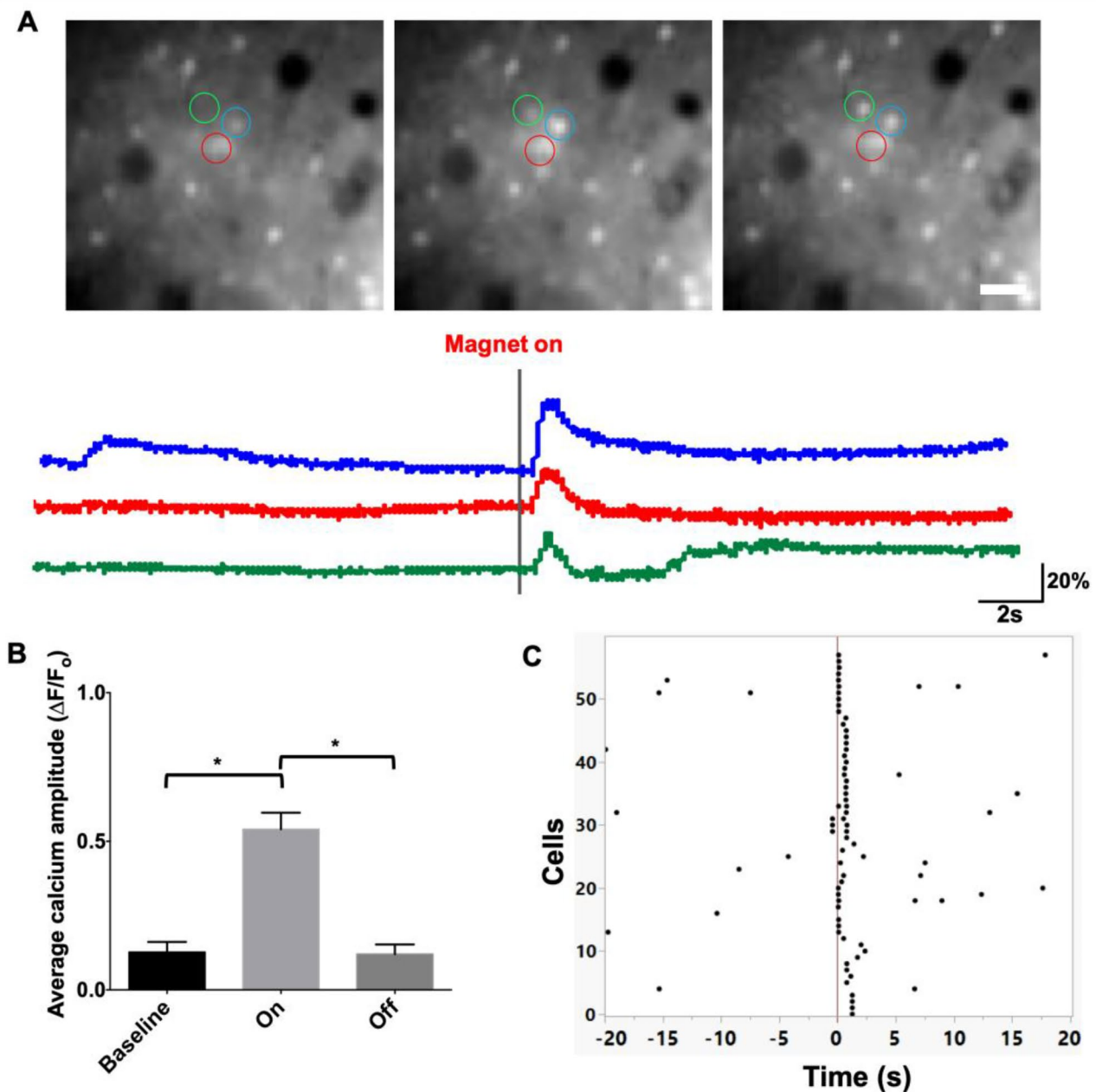
Fig. 2 Single unipolar magnetic pulses induced neuronal activity in MENs -loaded cortical slices. Cortical slices prepared from GCaMP6 transgenic mice were loaded with MENs similar to Fig. 2 and stimulated with single pulses of magnetic field (~750–875 Oe at 200 ms pulse-width). **A** Sample images of neurons in a slice and traces of calcium transients measured from the circled neurons. **B** Average peak amplitudes of calcium spikes measured at baseline and after the magnets were turned on and off. **C** Temporal response profile of all responding cells. Scale bar: 50 μm, *$p < 0.005$, $F = 32.86$, repeated-measured ANOVA, Tukey's HSD. $n = 13$ slices (total 4 animals)
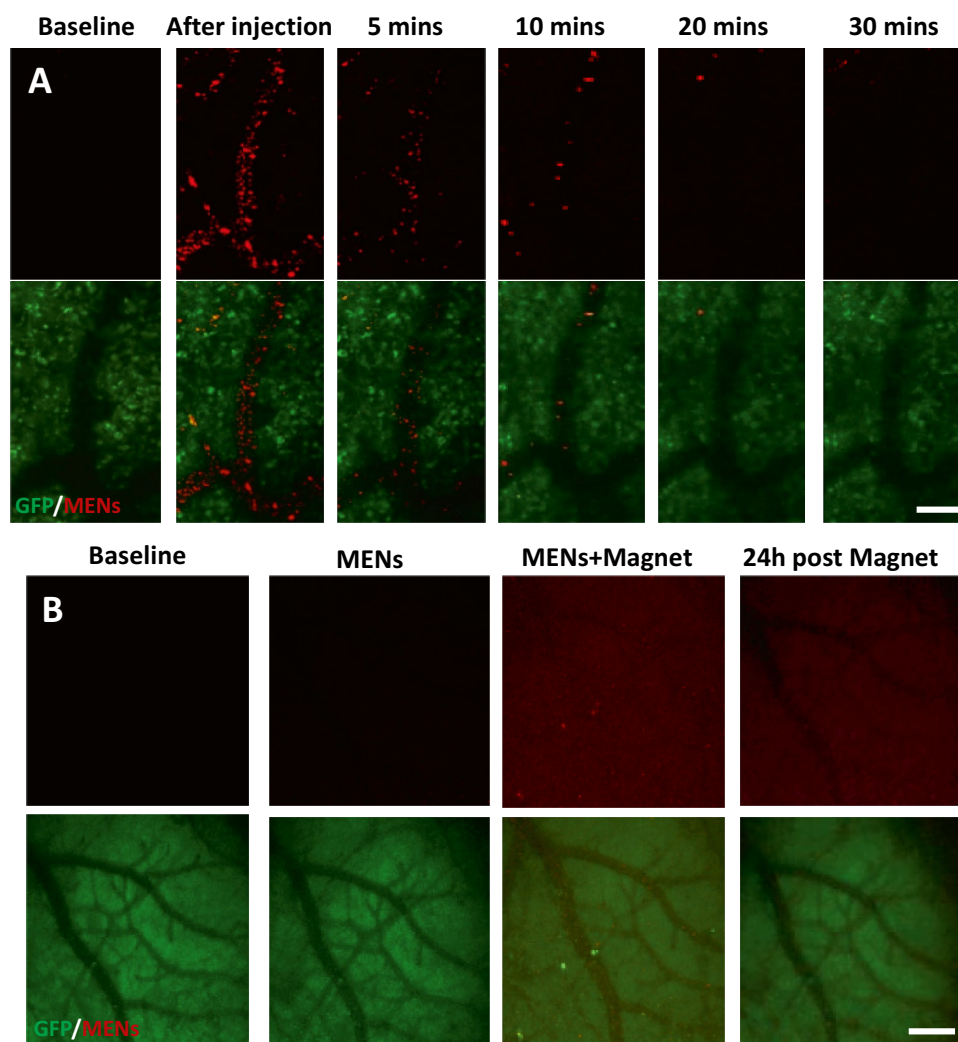
amplitude at the epicenter and gradual reduction in amplitude ($p < 0.05$, one-way ANOVA, Tukey's HSD, Fig. 6D, E, F) and an increase in the latency period (Fig. 6D, G, H) at locations further away from the epicenter. The results suggest that neuronal activity was initiated at the epicenter where MENs were localized and spread to more distal brain regions and the contralateral cortex. These data provide strong evidence that MENs-MS can activate neuronal activity in vivo.

MENs-MS Increased Cortical c-Fos Expression

We found an increase in cortical c-Fos expression only for animals that has both MENs delivery and MS, with an

Fig. 3 In vivo delivery of fMENs into mouse cortex. **A** Vascular MENs level reduced significantly after 10 min post injection. In vivo two-photon images of cortical blood vessels were taken at baseline (B.L.) and at 5, 10, 20, and 30 min after intravenous injection of 10 μg fluorescence labeled MENs (fMENs; top row **A**). No magnetic field was applied. Bottom row **A** represents cortical vasculature with green signal for GFP labeled neuron. Scale bar: 100 μm. **B** In vivo two-photon images of layer 2/3 sensorimotor cortex were taken at baseline (C1) and after (C2) intravenous injection of 10 μg fMENs, after applying ~4000–5000 Oe magnetic field for 45 min (C3), and on the second day after injection (C4) indicates successful delivery of MENs to cortical tissue after magnet application, which MENs remained up to at least 24 h after delivery (top row **B**). Bottom row **B** represents cortical layer 2/3 GFP neuronal signal. Scale bar: 100 μm

average of 176 ± 27.5 cells/counted region compare to 70.5 ± 15.25 for MENs only group and 51 ± 8 for MS-only group ($p < 0.05$, one-way ANOVA, Tukey's HSD, Fig. 7A, B). MENs only group and MS-only group had similar densities of c-Fos positive cells (Fig. 7A, B). The results further support that MENs-MS induced cortical neuronal activity in vivo.

MENs-MS Did Not Induce Astrogliosis and Microglial Activation

Delivering MENs to a specific brain region may initiate inflammatory responses of glial cells, particularly astrocytes and microglia (Fig. 8A–H). To assess whether astrogliosis and microglial activations occurred, we made intravenous injection of 200 μl of MENs at 200 μg/ml and magnetic delivery of MENs. Mice that received MENs delivery and MS were also assessed at various time point after the stimulation. We observed no significant differences in the densities of both IBA1 and GFAP positive cells among all

the groups (Fig. 8A–C, G, H). Considering these results together, MENs-MS did not induce any apparent inflammatory response in mice.

Discussion

We investigated the effects of MENs-MS for non-invasive activation of cortical neurons ex vivo and in vivo. By applying an external magnetic field, we non-invasively delivered MENs across the BBB to the brain and wirelessly stimulated cortical neuronal activity with a short latency, great efficiency, and reliability, without causing detectable neuroinflammatory reaction in the brain.

We developed MENs with a true core–shell nanostructure in which the magnetic core is intrinsically coupled to the piezoelectric shell via almost perfect lattice matching (Fig. 1A). To the best of our knowledge, such nanostructures have been fabricated for the first time [18]. Enabling such matching is the key to maximizing the ME coefficient,
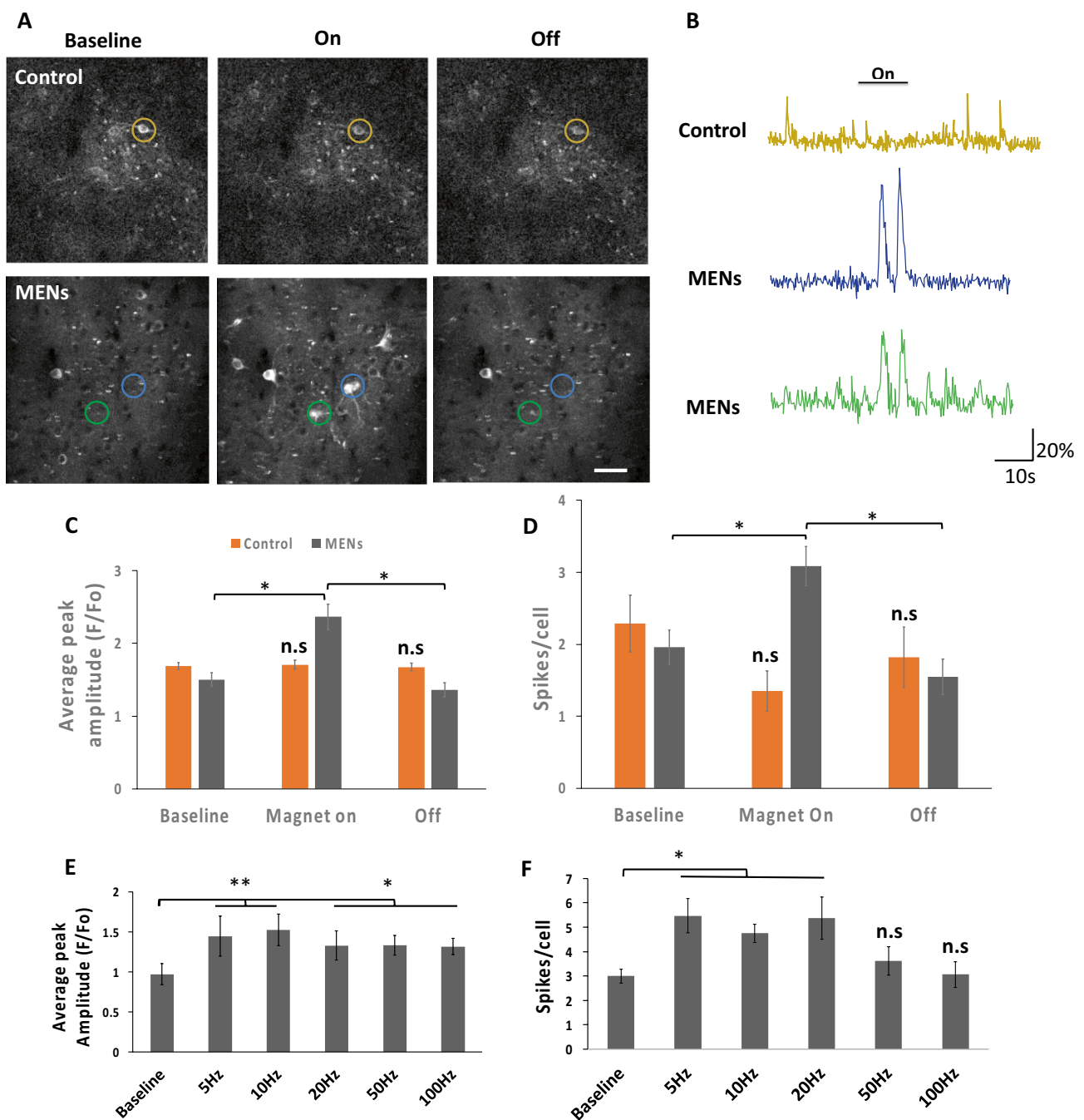
Fig. 4 Magnetic stimulation activated cortical layer II/III neuron in vivo. Representative images (**A**) and traces (**B**) of calcium transients measured from layer II/III cortical neurons. Mice of the control and MENs groups were injected with saline or MENs followed by permanent magnet application, respectively. Magnetic stimulation and imaging were identical for both groups. Significant increases in average calcium spike amplitude (**C**) and mean spike number (**D**) of cortical neurons after magnet stimulation was turned on only in MENs-treated animals. $n = 5$ mice, $*p < 0.05$, $F = 17.87$, one-way ANOVA, Tukey's HSD. Scale bar: 50 μm. Color of traces correspond to color of analyzed ROI. Increase in average calcium spike amplitude (**E**) and total spikes per cell (**F**) of cortical neurons when magnet was turned on at each frequencies of stimulations. Changes in the amplitudes and spike numbers of calcium transients at electromagnetic stimulation frequencies of 5, 10, 20, 50, and 100 Hz. The data indicate that magnetic waves between 5 and 10 Hz were most effective in stimulating neurons in vivo. $n = 5$, $*p < 0.05$, $**p < 0.01$, $F = 9.659$ two-way ANOVA, Tukey's HSD. Scale bar: 100 μm
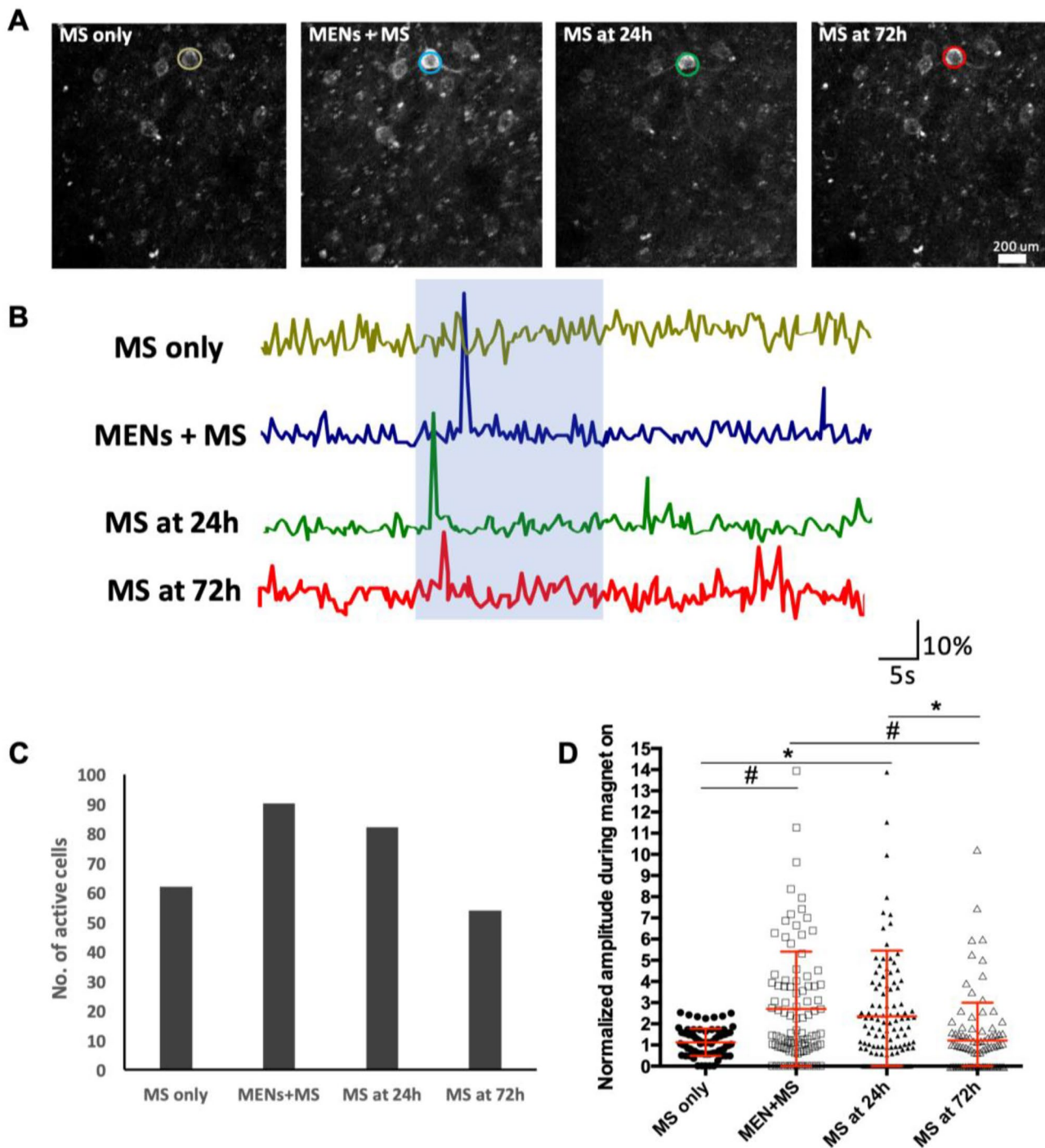
🖄 Springer

Fig. 5 MENs-MS was effective in activating neurons in 24 h after a single delivery of MENs. **A–B** Representative two-photon images and traces of calcium signals of same cortical layer II/III neurons at baseline (MS only) and immediately after MENs delivery followed by MS (MENs + MS), MS at 24 h after, and MS at 72 h after. A total of 10 Hz magnetic stimulation was applied for 20 s in the middle of recording period at each time point. **C** There was an increase in number of active neurons after MENs-MS, which remained higher up to 24 h after initial delivery. **D** There were increases in response amplitude immediately after MENs-MS and at least 1 day after initial delivery, which returned to baseline level at 3 days post-MENs delivery, one-way ANOVA, Tukey's HSD, $n = 5$, *$p < 0.05$, #$p < 0.005$, $F = 10.23$

which in turn is the most important feature of these nanoparticles enabling the creation of an efficient nanotransducer to activate neurons. The small size, on the order of 30 nm,

is important not only for their easy penetration through the blood–brain barrier (BBB) but also for ensuring that these nanoparticles can be precisely placed close or directly on
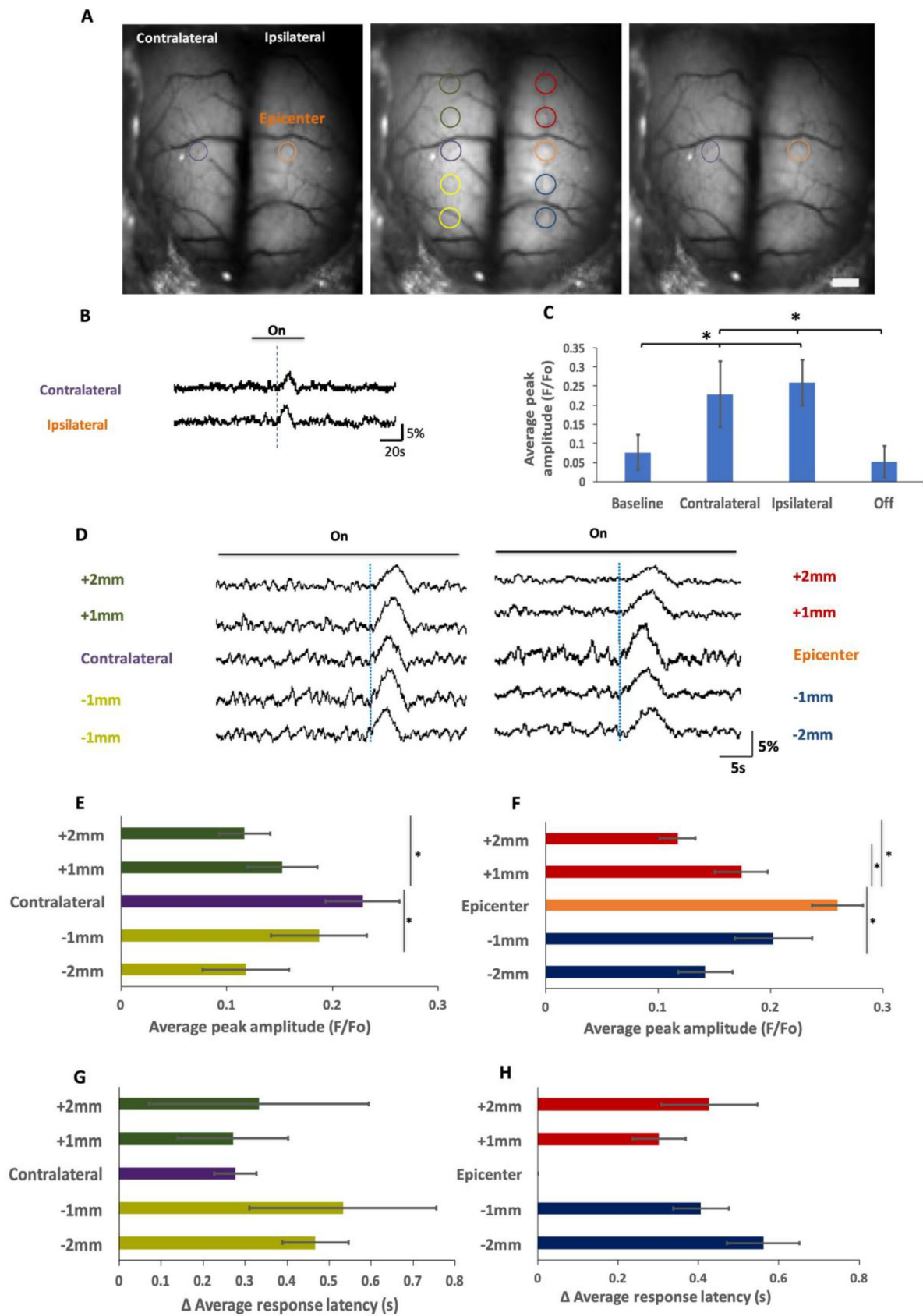
◀**Fig. 6** Mesoscopic activity imaging revealed initiation and spreading of MENs-MS induced cortical activity in vivo. Representative images (**A**) and traces (**B**) of calcium transients measured from both hemispheres at baseline (left image) and after turning on and off magnetic stimulation (middle and right images). The epicenter was a cortical region where a conical magnet was applied to attract MENs. Dotted lines indicate the start of calcium spike. **C** There were significantly higher amplitudes of calcium signals on cortex ipsilateral (at epicenter region) and contralateral (same region on opposite hemisphere) to MENs delivery induced by MS (10 Hz at 450 Oe for ~ 30 s). $n = 5$, *$p < 0.05$, $F = 12.18$, repeated-measured ANOVA, Tukey's HSD. **D** Sample traces of calcium transients measured from epicenter, cortical regions anterior and posterior from epicenter, and areas of contralateral cortex. **E, F** The mean amplitude of calcium signals in the epicenter was higher than that of cortical regions more anterior or posterior to it; the contralateral cortex had similar differences. **G, H** The latency period at the epicenter was the shortest than all other cortical regions. $n = 5$, *$p < 0.05$, $F = 36.29$, one-way ANOVA, Tukey's HSD. Scale bar: 1 mm

the neuronal membrane for maximizing their stimulating capabilities.

Because magnetic stimulation using a pair of electromagnets generates a high level of electromagnetic noise, we used calcium imaging techniques to record neuronal activities instead of using electrophysiological recording. Calcium imaging allowed us to efficiently examine neuronal activities not only in individual neurons but also in both cortical hemispheres. Upon magnetic application, we observed dramatic increases in neuronal calcium response after a short latency, with about one third of responses having a latency period of < 150 ms. Since calcium imaging signals are slower than electrical signals and GCaMP6 signal has a temporal resolution of 100–150 ms [21], the actual latency is estimated to be 50 ms and less. This is a good temporal resolution and a clear indication of the stimulatory effects of MENs on neuronal activity. Our observation of only ~ 33% of neurons having quick response time (i.e., latency of < 150 ms) could be due to at least two factors. One is the variabilities in the distribution of the MENs relative to the imaged neurons, which affects the efficacy of the MENs in changing membrane potential and causing neuronal firing. The other is the different and fluctuating excitability of the neurons in a given imaging region as determined by their instantaneous membrane properties and synaptic input; more excitable neurons will have short latency for activation. There were significant increases in both calcium transient amplitude and spike number only when the magnet was turned on. Furthermore, the increases in calcium transient amplitude were seen at all the tested frequencies of magnetic stimulation. Frequencies of calcium response were also elevated, but significant increases were observed only seen at 5, 10, and 20 Hz of magnet fields.

For in vivo brain stimulation, we first demonstrated that the MENs could be non-invasively delivered to brain parenchyma through intravenous injection followed by application of a permanent magnet on a target region of the skull. The transient existence of fMENs in the blood stream for < 30 min suggests that an effective time window for magnetic delivery of MENs lasted only for < 30 min. The MENs could be drawn across the BBB and localized to a region of the cortical hemisphere where the magnetic field was applied over the skull; the nanoparticles remained in the brain tissue for at least 24 h after the delivery. Earlier reports have shown that the delivered MENs appear to be localized mainly in the extracellular space both in CSF [22] and binding to extracellular membranes of various type of CNS residential cells [14, 22]. However, MENs are also found to be distributed in cell cytosol [22]. The chemical structure and integrity of MENs are not compromised during the process of navigation from the blood stream across the endothelial cell layers of the BBB to be localized in the brain [22]. We also found that the stimulatory effect of MENs lasted for at least 1 day after a single treatment and dissipated within 3 days. This result suggests the majority of the delivered MENs are cleared from the brain within 3 days, which may reduce potential side-effects or toxicity of the MENs. However, to achieve repetitive brain stimulation over a longer period, additional MENs delivery or modification of the MENs will be required to improve their retention. The whole brain mesoscopic imaging revealed activity changes in a spatially dependent manner relative to the location of MENs, suggesting that targeted stimulation of a brain region can be achieved by delivering MENs to a focal brain region defined by the strength of a magnetic field gradient.

One of the major hurdles in nanoparticle-based treatment techniques is the potential toxicity in vivo due to nanoparticle agglomerations (e.g., aggregations), which could induce toxicity and inflammation that may lead to abnormal gene expression, tissue degeneration, and cell death [23–25]. We coated the surface of MENs with a water-dispersible glycerol mono-oleate (GMO) to prevent aggregates and increase membrane crossing capability [26, 27] and found no significant changes in microglial activation nor astrogliosis up to 1 week after MENs delivery and magnetic stimulation. Consistently, Kaushik et al. also reported no changes in peripheral immune response, liver and kidney toxicity, and motor behavior up to 1 week after delivering MENs to the cerebral cortex [22]. Furthermore, the MENs produce no detectable toxicity on human astrocyte and peripheral blood mononuclear cells at a concentration of 0–200 μg/ml (~ 10 ug/kg MENs) [28]. Taken together, these results provide encouraging information on the safety of MENs to the body and brain in rodents and support its potential application for translational research and clinical treatment.

In addition to imaging neuronal activity, we also stained mouse cortical slices for c-Fos expression, a classical indicator of neuronal activity (e.g., action potential firing) [29,
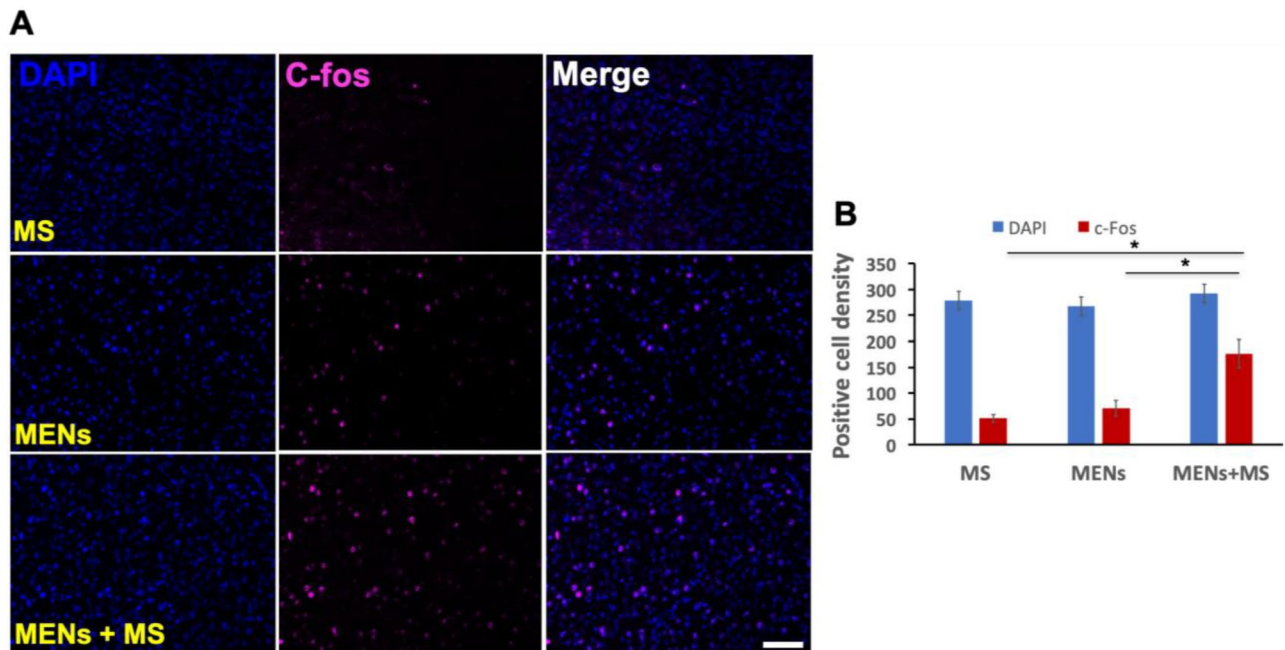
Fig. 7 MENs-MS increased the number of c-fos expressing cells. **A** Representative images of immunofluorescence from mice that received magnetic stimulation (MS, top row), MENs delivery only (middle row), or MENs+MS (bottom row). Images were taken with an 20×objective. **B** A significantly higher density of c-Fos expressing cells in MENs+MS group than either MS only or MENs only group. Scale bar: 20 µm. $n = 3$ mice/group, $*p < 0.05$, $F = 15.22$, Two-way ANOVA, Tukey's HSD

30], to confirm the stimulatory effect of MENs on neuronal activity histologically. c-*F*os is an immediate early gene that has low expression at basal level of activity. Upon repetitive action potential firing, Ca^{2+} influx results in a series of downstream signaling cascades involving calmodulin and CaMKII, which activates MAPK pathway to facilitate the expression of c-fos protein [30]. Thus, detecting the level of *c-Fos* expression can reflect the existence of enhanced neuronal activity. We found a significant increase in the number of cortical c-Fos expressing cells in MENs-MS animals. Although c-Fos expression in CNS is also observed in some activated astrocytes in inflammatory disease models [31, 32], our result of no increase in the number of activated astrocytes (Fig. 8) suggests that the increased number of c-Fos positive cells is likely activated neurons, which provides histological evidence supporting the effect of MENs-MS on activating neurons. Taken together, these results demonstrate a ground-breaking ability of MENs to enable wireless control of neuronal activity.

Our goal of this study was to demonstrate as a proof-of-concept the ability of MENs to be localized in a brain region and efficiently evoke neuronal activity. Additional research is needed to precisely deliver MENs to a focal region of the brain and to achieve cell-type specific activation. One approach would be to conjugate MENs with an antibody against a cell membrane protein so that the MENs can be targeted to a specific cell type or a subcellular component.

For the past two decades, there have been efforts to enhance delivery of substances, including metal-based magnetic nanoparticles, across the BBB [33–35]. One popular way that has been used widely both in research and in clinical application is pre-treatment with BBB-opening compounds such as mannitol [36] and borneol [37]. Combining these two approaches will help increase MENs delivery to the brain in a more specific manner.

In contrast to current non-invasive brain stimulation techniques, brain stimulation based on MENs offers a contactless and more efficient approach to modulate brain activity without the need of genetic modification. This technology has the potential to be a next frontier in non-invasive neuromodulations for studying neurophysiology and neural circuitry in humans and animal models and for both diagnosis and treatment of different neurological diseases such as chronic pain, epilepsy, Parkinson's disease, and Alzheimer's disease etc. With further optimizations of MENs delivery and cell- and region-specific targeting, this technology could potentially open a door to a more robust and precise brain control that currently is not possible.

In conclusion, this study demonstrates the ability of using MENs to wirelessly activate cortical neurons and cortical network ex vivo and in vivo. We have shown that MENs can be guided to penetrate the BBB to enter brain parenchyma under a magnetic field and have defined the effective time window and parameters for the delivery. Our ex vivo
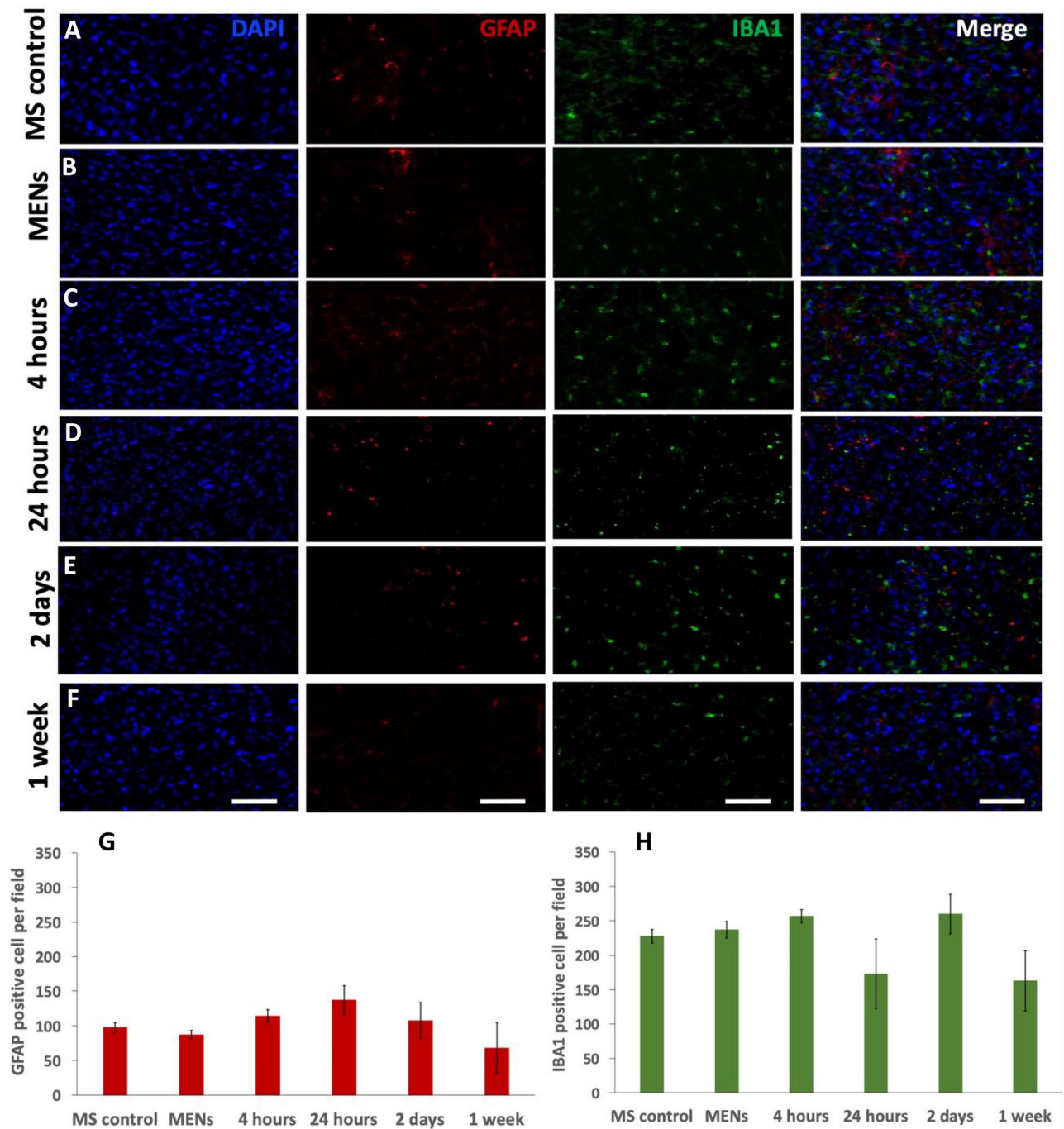
Fig. 8 No significant changes in the numbers of GFAP and IBA1 positive cells after MEN delivery and MENs-MS. Brain sections were obtained from six groups of C57BL mice including MS control, MENs-delivery (MENs), and MENs delivery followed by MS at 4 h, 24 h, 2 days, and 1 week after. **A–F** Sample confocal images of coronal cortical slices stained for DAPI, GFAP, and IBA1 at different time points. Quantifications of GFAP (**G**) and IBA1 (**H**) positive cells showed no significant differences in the numbers of these cells after MENs delivery or followed by MS. $n = 4$ mice/group. Scale bar: 50 μm

and in vivo calcium imaging data support that MENs-MS evoke cortical neuronal activity with fast temporal resolution at cellular and global network levels. Furthermore, the process of MENs delivery and magnetic stimulation did not

induce detectable neuroinflammation. In contrast to current non-invasive brain stimulation techniques, brain stimulation based on MENs offers a contactless, reliable, and efficient approach to modulate brain activity without the need of

genetic modification. With further optimizations of MENs delivery and cell- and region-specific targeting, this technique could potentially open a door to a more robust and precise brain control that currently is not possible.

Materials and Methods

MENs Synthesis, Ultrastructural Imaging, and Functionalization

MENs were synthesized using a standard method as described in Wang et al. [18]. We developed MENs with a core–shell nanostructure, in which the magnetic core was intrinsically coupled to the piezoelectric shell via perfect lattice matching (Fig. 1). The size of the MENs was on the order of 30 nm. With this new synthesis, we were able to develop MENs with a high ME coefficient of > 5 V/cm/Oe in the frequency range, 0 to 200 Hz, under study. The details of this study have been presented in a recent publication [18]. Samples for transmission electron microscope (TEM) imaging were prepared by dispersing 1 mg MENs in 2 mL ethanol and sonicating the mixture for 20 min. One drop of the MENs solution was deposited with a pipette on a copper TEM grid substrate. Slowing evaporation at low temperature provided a uniform nanoparticle distribution on the substrate.

To eliminate aggregation and potential toxicity, the surfaces of the MENs were functionalized by adding a 2-nm-thick coating of glycerol mono-oleate (GMO) as follows: the MENs were washed twice with phosphate-buffered saline (PBS, pH 7.4) and sonicated for 2 min between washes for uniform dispersion in solution. MENs were then suspended in a GMO solution (8 μL GMO/1 g MENs) and mixed thoroughly on a rotator for 12 h. Excess GMO were then removed by extraction with 1 ml of 70% ethanol: PBS and two subsequent washes with PBS. Finally, the MENs-GMO mixture were suspended in saline and stored at -20 °C for short-term storage of 3–5 days or freeze-dried in liquid nitrogen for long-term storage for more than 1 week. To prepare fluorescent MENs (fMENs), Texas Red NHS ester was first reacted with oleylamine (2:1 molar ratio) for 18–24 h on a rotator in a dark environment. Then, hexane was added in drops incrementally to help dissolved the oleylamine-Texas Red mixture. After the solution of oleylamine-Texas Red NHS ester was combined with the GMO-MENs mixture (1:3 volume ratio of GMO-MENs: oleyamine-TexasRed), it was rotated for additional 12 h to allow binding. Following removal of excess GMO through multiple washes in PBS, the final product of concentration 5 mg/mL (MENs/GMO-to-PBS) was store at -20 °C (short-term storage).

Magnetic Characterization of Nanoparticles: A Lake Shore alternating gradient magnetometer (AGM) system, with a 10^{-6} emu sensitivity, was used to measure the M-H loops of the nanoparticles at room temperature. The ME coefficient versus the applied a.c. magnetic field strength and frequency was measured using a nanoprobe setup, discussed in our earlier publication [18].

Ex Vivo Imaging of Cortical Slices from GCaMP6s Transgenic Mice

All experiments were approved by the Institutional Animal Care and Use Committee (IACUC) of the Indiana University School of Medicine, which are in accordance with National Institutes of Health guidelines for the care and use of laboratory animals. Thy1-GCaMP6 transgenic mice were purchased from the Jackson's Laboratory and bred locally. Cortical slices were prepared from Thy1-GCaMP6 transgenic mice that were 20–22 days old ($n = 5$). After the animals were anesthetized, the brain was removed and coronal cortical slices of 350 μm thick were cut using a vibratome (VT1200, Leica Biosystems, Buffalo Grove, IL.) The slices were then collected and incubated in an oxygenated aCSF solution (126 mM NaCl, 2.5 mM KCl, 2 mM $MgSO_4$, 1.25 mM NaH_2PO_4, 26 mM $NaHCO_3$, 2 mM $CaCl_2$, 10 mM D-Glucose) at room temperature.

Magnetic Field Application: Prior to imaging, a brain slice was placed in a custom-made recording chamber filled with 37 °C aCSF. The recording chamber was a 2-cm diameter well with a glass bottom that was filled with aCSF containing 5 μL of MENs (5 mg/mL). A 5000 Oe conical magnet was used to apply a strongly localized magnetic field to the bottom of the chamber for approximately 15 min to draw the MENs to a small area of the slice. For magnetic stimulation, two electromagnets were put on opposite sides of the recording chamber in a Helmhotz pair arrangement according wherein the diameter of each coil was comparable to the separation between the coils. This arrangement was chosen to significantly reduce or eliminate a magnetic force to ensure the nanoparticles did not physically move during the stimulation process. A unipolar magnetic field of 750–875 Oe with 200 ms pulse-width was applied during the imaging process.

Calcium Imaging: A recording chamber was made by attaching a temperature control heated well (Thermal Well Temperature Controller TC-100, BioScience Tools, San Diego, CA) onto a coverslip. A cortical slice was placed in the chamber, and calcium activities were imaged with a Leica DM6000 FS upright microscope. Images were capture with an iXON EMCCD DU-88U camera system (Andor USA, Concord, MA) at ~45–50 fps. Cortical slices were imaged at ~35 °C in aCSF with 20 μM bicuculline.

In Vivo Two-Photon Imaging of fMENs in Cerebral Blood Stream and After Delivery

Thy1-GCaMP6 mice ($n=5$) were anesthetized with Keta-mine/Xylazine mixture (87.3 mg/kg/13.7 mg/kg), and the scalp was removed. A cranial window (3 mm in diameter) was made in an area 1.5-mm lateral from the midline and 1 mm posterior from the bregma. After the animals were allowed to recover for 7 to 10 days, a single injection of 200 µl of fMENs at 200 µg/ml was made through the retro-orbital route. Two-photon images of cerebral blood vessels were taken at baseline, and 0, 5, 10, 20, and 30 min after fMENs injection. Video series of MENs with blood flow are stacked to generate a single image for each time point.

Two-photon imaging: Two-photon imaging of corti-cal slices was performed using a Prairie Technologies Ultima 4423 two-photon system (Bruker Inc., Middleton, WI) equipped with a MaiTai Ti: Sapphire laser (Newport, Mountain View, CA) tuned to 900 nm. Band-pass filtered fluorescence (560–600 nm) was collected by photomultiplier tubes of the system. The average laser power on the sample was $\sim$20–30 mW. All images were acquired at a resolution of 512×512 pixels using a $20 \times$ water-immersion objective (Nikon Instruments Inc., Melville, NY). Images were capture at a rate of 4–5 fps.

MENs delivery: For imaging MENs delivery, GCaMP6 mice with cranial windows received an injection of 200 µL fMENs at 5 mg/ml. After two sets of stacked cylindrical magnets of 6000 Oe field strength were separately placed on top of the cranial window and beneath the mouth of the mouse for 10 min, a conical magnet with the field of 5000 Oe at the tip was applied to the cranial window to further localize the MENs. Images were taken before and after fMENs injection, after fMENs injection with magnet application, and 24 h after MENs delivery.

In Vivo Two-Photon Calcium Imaging of Cortical Neurons in GCaMP6 Transgenic Mice

Mice with cranial windows prepared as described above were used in this experiment. After the animals were sedated via 4% isoflurane and maintained with chlorprothixene (0.04 mg/ml, i.p.), they were separated into a saline-treated control group and an MENs-treated group and received retro-orbital injection of 200 µl of saline or 200 µl of MENs at 5 µg/ml, respectively. After the application of permanent magnets as described above to both groups for MENs delivery, the animal's head was stabilized by fixing the L-shaped titanium metal plate to a custom-made base and the body temperature was maintained. Magnetic stimulation was made by placing two electromagnets ($\sim$500 ms pulse-width at $\sim$300–450 Oe) closely on both side of the head. Again, the Helmholtz pair arrangement of the electromagnet was chosen to minimize

the pulling magnetic force on the nanoparticles during the stimulation events.

Two-Photon Imaging: Two-photon imaging of corti-cal slices was performed using a Prairie Technologies Ultima 4423 two-photon system (Bruker Inc., Middleton, WI) equipped with a MaiTai Ti: Sapphire laser (Newport, Mountain View, CA) tuned to 900 nm. Band-pass filtered fluorescence (560–600 nm) was collected by photomultiplier tubes of the system. The average laser power on the sample was $\sim$20–30 mW. All images were acquired at a resolution of 512×512 pixels using a $20 \times$ water-immersion objective (Nikon Instruments Inc., Melville, NY). Two-photon images of calcium transients were taken at baseline and during and after magnetic stimulation. In each imaging field, two optical planes in layer II/III were imaged for 2 min at 4–5 frames per second (fps). Typically, each recording session consisted of 30 s of baseline recording, 40 s with magnetic field application, and 30 s of post-magnetic application period. We tested a combination of different stimulation frequencies (5, 10, 20, 50, and 100 Hz).

Mesoscopic Calcium Imaging of Cortical Activity In Vivo

Thy1-GCaMP6 transgenic mice were anesthetized with Ket-amine/Xylazine mixture (87.3 mg/kg/13.7 mg/kg), and the scalp was removed. After a large cranial window (approximately 10×8 mm) was made by removing the skull, a piece of curved cover glass was installed and tightly sealed with super glue and dental cement. The animals were allowed to recover for 7 to 10 days prior to imaging. A mesoscopic imaging set-up was built similar to previously described method [38, 39]. Images were captured with a two-lens system composed of a top zoom Nikkor 70–300 mm lens of aperture f3.5–5.6 set at 70 mm at f3.5 coupled with an inverted lens adapter to a bottom Nikkor 50 mm prime lens at f1.4. Videos were captured with an iXON EMCCD DU-88U camera system (Andor USA, Concord, MA) controlled by MetaMorph software. Delivery of MENs and magnetic stimulation paradigm were done exactly as described in two-photon imaging.

Data Analysis of Ca Imaging

Two-photon imaging data were analyzed using ImageJ soft-ware (NIH) with a Time Series Analyzer plugin (Balaji J. UCLA). All active cells within each frame were analyzed. To analyze individual cells, three separate background points were chosen by drawing circles with the same diameter as the respective cell body in the surrounding area. For mesoscopic brain imaging, a circular area of interest ($\sim$1 mm in diameter) was selected, with an adjacent blood vessel selected as background to compensate for changes in

general brightness. The fluorescence calcium signal of a cell $\Delta F/F$ was calculated by Eq. (1) excerpt from Chen et al. [21] that was developed by Kerlin et al. [40]:

$$\frac{\Delta F}{F} = \frac{\left(F_{true} - F_B\right)}{F_B} \text{ and } F_{true} = F_{cell} - r * F_B \quad (1)$$

where F_B is the average baseline fluorescence over three different regions surrounding the cell of interest and r is the contamination ratio standard constant 0.7. The data were then used to construct a calcium peak profiles using Origin-Pro 9.1 (OriginLab, Northampton, MA). Analyses of peak amplitude, frequency, and durations were done with Peak analysis toolbox of OriginPro 9.1.

C-fos Staining of Cortical Neurons

C57BL6J mice ($n = 4$ animals/group) were assigned into three groups: control (saline injection + MS (5×2 min MS at 10 Hz)), MENs (MENs delivery without magnetic stimulation), and MENs-MS (MENs delivery and MS (5×2 min MS at 10 Hz)). MENs delivery and magnetic stimulation (MS) were done similarly as described above.

Brain tissues were stained for c-Fos protein, an indicator of action potential firing [29]. Four hours after the treatment, the mice were deeply anesthetized and perfused transcardially with PBS buffer, followed by 4% formaldehyde PFA at room temperature. The brains were then dissected and placed in 30% sucrose for 48–72 h at 4 °C. The tissue was then frozen and sectioned with a cryostat at thickness of ~45 μm. Immunofluorescence was performed on free-floating sections by incubating overnight with a primary antibody for c-Fos (rabbit; 1:800, Sigma Aldrich G3893) and followed by incubation with fluorescent goat anti-rabbit secondary antibody (1:200; Invitrogen, Carlsbad, CA). For nuclear staining, 4′, 6-diamidino-2-phenylindole (DAPI; 1: 10,000) was added to the solution for a final 5 min. Finally, slices were imaged using a Neurolucida imaging system.

Immunofluorescence Analysis of Astrocytes and Microglia

To determine potential glial reactivity and neuroinflammation induced by the MENs, we used an antibody against ionized calcium binding adaptor protein (IBA1) to label microglia, and an antibody against Glial Fibrillary Acidic Protein (GFAP) to label astrocytes [41, 42]. C57BL6J mice were divided into three groups: control (saline + MS), MENs (MENs without MS), and MENs-MS (MENs delivery with MS). The MENs delivery and MS paradigm were identical to the c-Fos experiment described above. Within the MENs-MS group, subgroups of mice were euthanized at 4 h, 24 h, 3 days, or 1 week after MS. Mice were perfused, and brain

slices were stained as described above. Anti-GFAP (mouse; 1:800, Sigma Aldrich G3893) and anti-IBA1 (goat; 1:200, ABCam ab5076) antibodies were followed by secondary antibodies of goat anti-mouse Cy5 (1:500, Jackson Immuno) and donkey anti-goat 488 nm (1:1000, Fischer Scientific).

Statistics

All statistical analyses were done with Jmp Analysis 11 and GraphPad Prism 6. Repeated measure ANOVA or one-way ANOVA were used for analyses of calcium signals and immunohistochemical data. For comparisons that yielded statistical significances, Tukey's HSD post hoc analyses were applied for further comparisons between specific groups.

Declarations

Conflict of Interest The authors declare no competing interests.

References

1. F. e. a. Hummel, Effects of non-invasive cortical stimulation on skilled motor function in chronic stroke. *Brain* **128**, 164–174 (2005).
2. C. e. a. Miniussi, Efficacy of repetitive transcranial magnetic stimulation/ transcranial direct current stimulation in cognitive neurorehabilitation. . *Brain Stimulation* **1**, 326–336 (2008).
3. A. Demirtas-Tatlidede, ..., A. Pascual-Leone, Non-invasive brain stimulation in traumatic brain injury. *Journal of Head trauma rehabilitation* **27**, 274-292 (2012).

4. T. Wagner, Valero-Cabre, A., Pascual-Leone, A., Noninvasive human brain stimulation. *Annual Review of Biomedical England* **9**, 527–565 (2007).

5. N. Sollmann, Hauck, T., Tussis, L., Ille, S., Maurer, S., Boeckh-Behrens, T., Ringel, F., Meyer, B., Krieg, S.M., Results on the spatial resolution of repetitive transcranial magnetic stimulation for cortical language mapping during object naming in healthy subjects. *BMC Neuroscience* **17**, (2016).

6. R. Sparing, Mottaghy, F.M. , Noninvasive brain stimulation with transcranial magnetic or direct current stimulation (TMS/tDCS)-From insights into human memory to therapy of its dysfunction. *Methods* **44**, 329–337 (2008).

7. A. R. Brunoni, Nitsche, M.A., Bolognini, N., Bikson, M., Wagner, T., Merabet, L., Edwards, D.J., Valero-Cabre, A., Rotenberg, A., Pascual-Leone, A., Ferrucci, R., Priori, A., Boggio, P.S., Fregni, F., Clinical research with transcranial direct current stimulation (tDCS): challenges and future directions. *Brain Stimulation* **5**, 175-195 (2012).

8. T. K. Gradinaru V., Zhang F., Mogri M., Kay K., Schneider B., Deisseroth K., Targeting and readout strategies for fast optical neural control in vitro and in vivo. *Journal of Neuroscience* **27**, 14231–14238 (2007).

9. L. Fenno, Yizhar, O., Deisseroth, K. , The development and application of Optogenetics. *Annual Review of Neuroscience* **34**, 389–412 (2011).

10. R. Chen, G. Romero, M. G. Christiansen, A. Mohr, P. Anikeeva, Wireless magnetothermal deep brain stimulation. *Science* **347**, 1477-1480 (2015).

11. H. Huang, Delikanli, S., Zeng, H., Ferkey, D.M., Pralle, A., Remote control of ion channels and neurons through magnetic-field heating of nanoparticles. *Nature Nanotechnology* **5**, 602–606 (2010).

12. A. Bystritsky, Korb, A. S., Douglas, P. K., Cohen, M. S., Melega, W. P., Mulgaonkar, A. P., et al. , A review of low-intensity focused ultrasound pulsation. *Brain Stimulation* **4**, 125–136 (2011).

13. K. Yue *et al.*, Magneto-electric nano-particles for non-invasive brain stimulation. *PloS one* **7**, e44040 (2012).

14. R. Guduru *et al.*, Magnetoelectric 'spin' on stimulating the brain. *Nanomedicine (Lond)* **10**, 2051-2061 (2015).

15. J. A. Kozielski K., Gilbert H., Yu Y., Erin O., Francisco D., Alosaimi F., Temel Y., Sitti M., Injectable nanoelectrodes enable wireless deep brain stimulation of native tissue in freely moving mice. *BioRivx*, (2020).

16. P. M. e. al., Size-dependent intranasal administration of magnetoelectric nanoparticles for targeted brain localization. *Nanomedicine: Nanotechnology, Biology, and Medicine* **32**, (2021).

17. E. Burgess, M. Sylvester, …, M. M. Boggiana, Effects of Transcranial Direct Current Stimulations (tDCS) on Binge-eating disorder. *International Journal of Eating Disorders* **49**, 930-936 (2016).

18. P. Wang *et al.*, Colossal Magnetoelectric Effect in Core-Shell Magnetoelectric Nanoparticles. *Nano Lett* **20**, 5765-5772 (2020).

19. D. T. Ping Wang, Elric Zhang, Mackenson Telusma, Dwayne McDaniel, Ping Liang, Sakhrat Khizroev., Scanning probe microscopy study of cobalt ferrite-barium titanate coreshell magnetoelectric nanoparticles. *Journal of Magnetism and Magnetic Materials* **516**, (2020).

20. e. a. Wang P., Colossal Magnetoelectric Effect in Core-Shell Magnetoelectric Nanoparticles. *Nano Letter* **20**, 5765–5772 (2020).

21. T. J. W. Tsai-Wen Chen, Yi Sun, Stefan R. Pulver, Sabine L. Renninger, Amy Baohan, Eric R. Schreiter, Rex A. Kerr, Michael B. Orger, Vivek Jayaraman, Loren L. Looger, Karel Svoboda, Douglas S. Kim, Ultrasensitive fluorescent proteins for imaging neuronal activity. *Nature* **499**, (2013).

22. A. Kaushilk, M. Nair et al., Magnetically guided central nervous system delivery and toxicity evaluation of magneto-electric nanocarriers. *Scientific Reports* **6**, (2016).

23. S. W. Lankoff A., Wegierek-Ciuk A., Lisowska H., Refsnes M., Sartowska B., Schwarze P., Meczynska-Wielgosz S., Wojewodzka M, Kruszewski M., The effect of agglomeration state of silver and titanium dioxide nanoparticles on cellular response of HepG2, A549 and THP-1 cells. . *Toxicology Letters* **208**, 197–213 (2012).

24. F. E, The role of surface charge in cellular uptate and cytotoxicity of medical nanoparticles. *International Journal of Nanomedicine* **7**, 5577–5591 (2012).

25. T. S. Okuda-Shimazaki J., Kanehira K., Sonezaki S., Taniguchi A., Effects of Titanium Dioxide nanoparticle aggregate size on gene expression. *International Journal of Molecular Science* **11**, 2383–2392 (2010).

26. M. Nair, Guduru R., Liang P., Hong J., Sagar V., Khizroev S., Externally ocntrolled on-demand release of anti-HIV drug using magneto-electric nanoparticles as carriers. *Nature Communications* **4**, (2013).

27. S. A. Dilnawaz F., Mewar S., Sharma U., Jagannathan N.R., Sahoo S., The transport of non-surfactant based paclitaxel loaded magnetic nanoparticles across the blood brain barrier in a rat model. *Biomaterials* **33**, 2936–2951 (2012).

28. A. Kaushik, Jayant, R., Nikkhah-Moshaie, R. et al., Magnetically guided central nervous system delivery and toxicity evaluation of magneto-electric nanocarriers. *Scientific Reports* **6**, (2016).

29. E. Bullitt, Expression of C-fos-Like Protein as a marker for neuronal activity following noxious stimulation in Rats. *Journal of Comparative Neurology* **296**, 517-530 (1990).

30. A. Hudson, Genetic reporters of neuronal activcity: c-Fos and GCamp6. *Methods Enzymology* **603**, 197-220 (2018).

31. Y. A. Wu B., Quercetin inhibits c-fos, Heat Shock Protein, and Glial fibrillary acidic protein expression in injured astrocytes. *Journal of Neuroscience Research* **62**, 730–736 (2000).

32. K. Y. Groves A., Jonnalagadda D., Rivera R., Kennedy G., Mayford M., Chun J., A functionally defined in vivo astrocyte population identified by c-Fos activation in a mouse model of multiple sclerosis modulated by S1P signaling: immediate-early astrocytes (ieAstrocytes). *eNeuro*, (2018).

33. L. P. Koziara JM, Allen DD, Mumper RJ., The blood-brain barrier and brain drug delivery. *Journal of Nanoscience Nanotechnology* **6**, 2712–2735 (2006).

34. Y. Z. Y. J. Yu, M. Kenrick, K. Hoyte, W. Luk, Y. Lu, J. Atwal, J. M. Elliott, S. Prabhu, R. J. Watts, M. S. Dennis. , Boosting brain uptake of a therapeutic antibody by reducing its affinity for a transcytosis target. *Science Translational Medicine* **3**, (2011).

35. J. Q. Qiao R., Huwel S., Xia R., Liu T., Gao F., Galla H., Gao M., Receptor-mediated delivery of magnetic nanoparticles across the blood-brain barrier. *ACS Nano* **6**, 3304–3310 (2012).

36. J. A. Chu C., Lesniak W., Thomas A., Lan X., Linville R. et al., Optimization of osmotic blood-brain barrier opening to enable intravital microscopy studies on drug delivery in mouse cortex. *Journal of Controlled Release* **317**, 312–321 (2020).

37. F. B. Zhang Q., Zhang Z. , Borneol, a novel agent that improves central nervous system drug delivery by enhancing blood-brain barrier permeability. *Drug Delivery* **24**, 1037–1044 (2017).

38. X. D. Silasi G., Vanni M., Chen A, Murphy T., Intact skull chronic windows for mesoscopic wide-field imaging in awake mice. Journal of Neuroscience Methods 267, 141-149 (2016).

39. D. Barson, Hamodi, A.S., Shen, X. et al., Simultaneous mesoscopic and two-photon imaging of neuronal activity in cortical circuits. *Nature Methods* **17**, 107–113 (2020).

40. M. A. A. Kerlin, V. Berezovskii, R.C. Reid, Broadly tuned response properties of diverse inhibitory neuron subtypes in mouse visual cortex. *Neuron* **67**, 858-871 (2010).

41. K. S. Imai Y., Intracellular signaling in M-CSF-induced microglia activation: role of Iba1. *Glia* **40**, 164–174 (2002).

42. E. W. Liedtke W., Bieri PL., Chiu FC., Cowan NJ., Kucherlapati R., Raine CS., GFAP is necessary for integrity of CNS white matter architecture and long-term maintenance of myelination. *Neuron* **17**, 607–615 (1996).